Ultrafast processes in nanooptics

There was significant progression in the research field of nanooptics and its applications in recent years [1-4]. Intense parallel development occurred in the investigation of ultrafast light-matter interaction processes on the nanoscale [5-6]. Along these lines, we and other research groups started to carry out the examination of ultrafast electron emission and electron acceleration in the nanolocalized and highly enhanced electromagnetic fields of propagating and localized surface plasmon polaritons (SPPs) or nanotips [7-10].

As a continuation of this research direction, in this project ultrafast photoemission near-field probing technique was developed [11] to investigate the fundamental question of plasmon–plasmon coupling and its effect on large field enhancement factors. By measuring and analyzing plasmon field enhancement values at different nanostructured surfaces based on the spectrally resolved electron emission measurements, it was possible to separate the contributions from propagating and localized plasmons (Figure 1). When resonance conditions are met, a significant field enhancement factor can be attributed to the generation of localized plasmons on surface nanostructures, acting as dipole sources resonantly driven by the propagating plasmon field. The coupling of propagating surface plasmon waves and localized plasmon oscillations in nanostructures is an essential phenomenon determining electromagnetic field enhancement on the nanoscale.
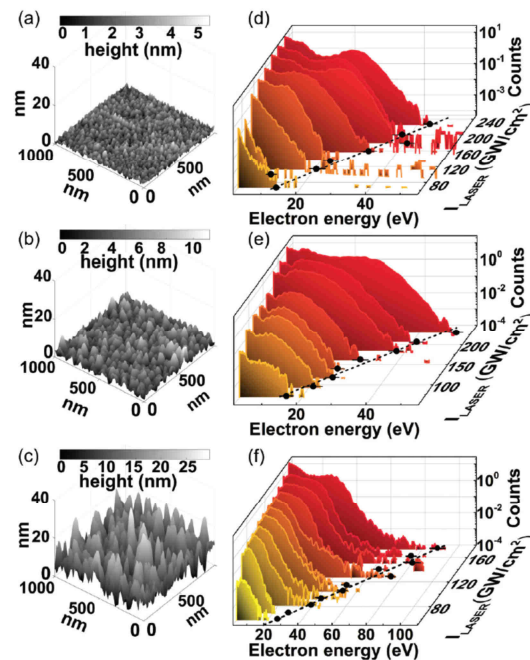

Figure 1. Surface morphology and the corresponding electron spectra. (a–c) Atomic force microscope scans of plasmonic surfaces with different rms roughness of 0.8 nm, 1.6 nm and 4.5 nm. (d–f) Plasmonic photoelectron spectra from the corresponding three surfaces by generating plasmons as a function of laser intemsity. The black symbols correspond to electron spectral cutoffs.

Moreover measurements were performed by a time of flight spectrometer investigating the surface plasmon-induced photoemission on the ordered sample [12]. During the sample preparation 100 nm dielectric spheres were deposited as an ordered structure by Langmuir-

Blodget method on a rectangular prism and it was covered by a 45-nm gold film for plasmon coupling. Oscillations with a certain period could be identified based on the measurements in the time of flight spectra, and furthermore narrower peaks were detected with shorter time periodicity. The possible interpretation of these peaks is the detection of high plasmon filed induced electron pairs, consistent with previous results [13-14]

Furthermore, the nanoscale control of plasmonic field enhancement was demonstrated experimentally by changing the polarization state of generating light [15]. Photoelectron emission from plasmonic nanorods was generated by illumination with linearly and circularly polarized femtosecond laser pulses. Determination of the field enhancement factor was achieved by our above mentioned ultrafast method based on the measurement of the kinetic energy spectra of photoelectrons accelerated in the plasmonic near-fields. [10-11]. The field enhancement factor of plasmonic nanorods was determined by these methods in the case of linearly and circularly polarized femtosecond laser pulses illumination. It was shown by electron trajectory calculations that the same acceleration mechanism and scaling law is valid for both polarization states of the excitation. Based on the numerical solution of Maxwell's equations the observed differences in field enhancement factors can be described by the mode-mixing property of circularly polarized illumination, meaning parallel excitation of multiple plasmon modes of the nanostructures. These experiments offer an ultrafast tool for manipulating the field enhancement property of nanostructures by changing the polarization state of light. These results have been already submitted to Applied Physics Letters journal. (see Appendix A for manuscript.)

In addition nonadiabatic tunneling in the transition region between the multiphoton emission and adiabatic tunnel emission is experimentally and theoretically investigated in fields of plasmonic nanostructures [16]. Spectrally resolved photoemission experiments were performed with a hemispherical energy analyzer between the regimes of multi-photon-induced photoemission and the nonadiabatic tunneling of electrons at the surface of metal nanoparticles with utilization the plasmonic nanometer-scale field localization and near-field probing at the same time. By analyzing the distinct plateau-like structures that appear in the photoelectron spectra, it was shown that in the transition region tunneling and rescattering of electrons take place at the same time when the electron current depends on the photocurrent. Measured electron spectral features in this transition region were well reproduced with the numerical solution of the time-dependent Schrödinger equation. The manuscript writing is already completed from these results and it will be submitted soon to Physical Review Letters. (see Appendix B for manuscript)

Finally, time-resolved autocorrelation experiments based on nonlinear electron emission from plasmonic nanoparticles were performed. Because multi-photon-induced emission takes place from gold and silver at the utilized 800 nm wavelength therefore this highly nonlinear process can be applied for constructing a nonlinear interferometric autocolerrator probing the local field with the help of photoelectrons. The characteristic emission mechanism is the three or four photon induced emission because of the work functions of the gold and the silver are around 5 eV and the photon energy is around 1.5 eV at 800 nm wavelength.
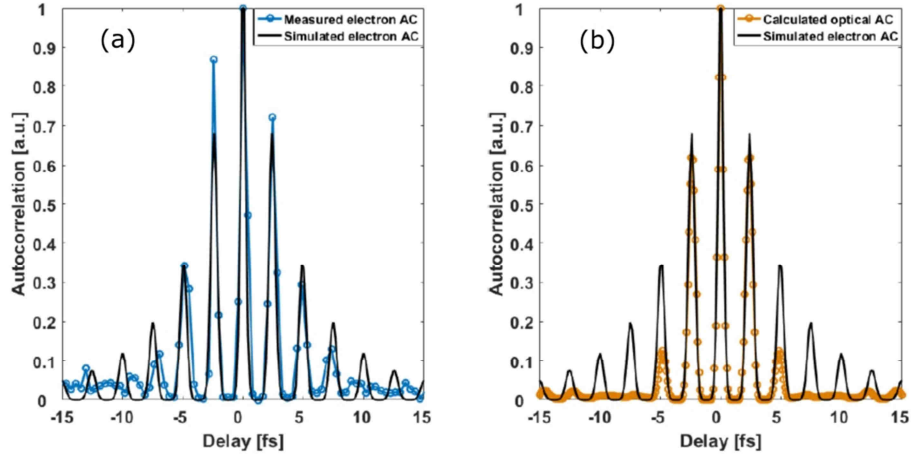
Figure 2. (a) Simulated and measured fourth order interferometric photoelectron autocorrelation traces. The signal is defined by the photoelectron current as a function of the delay. (b) Calculated optical autocorrelation of the exciting laser pulse and simulated electron autocorrelation showing that the plasmon autocorrelation broadens because of spectral filtering.

During this experiment the total plasmonic photocurrent can be measured as a function of the delay between the two arms of an ultrabroadband interferometer. Because the electron emission is determined by the plasmonic near field therefore the time evolution of the plasmon filed can be determined from this type of measurements. Based on the early measurements with ultrashort few optical cycle laser pulses (5,5 fs), short few cycle localized plasmon field can be generated. But the characteristic time evolution of plasmon near field is longer than pulse length of the generating optical filed because of spectral filtering caused by plasmon couplings (Figure 2)

Based on further measurement on rectangular nanoparticles, different plasmon pulse lengths could be demonstrated at different polarization excitations in accordance with different resonance frequencies depend on the characteristic lengths of the nanoparticles in different directions of the polarization. In addition, the autocorrelation measurements are also performed in energy resolution. The autocorrelations for a given electron energy range have become measurable (Figure 3). In this way, for example it is possible to study the time evolution of nanooptic field regions with the maximum field-enhancement, since the electrons with the maximum energy are emitted from these spatial regions, and consequently we may be able to make space and time resolved measurements. Further experiments are still ongoing and the first results have not yet been published in referred journal, but have already been presented at conferences [17-19].
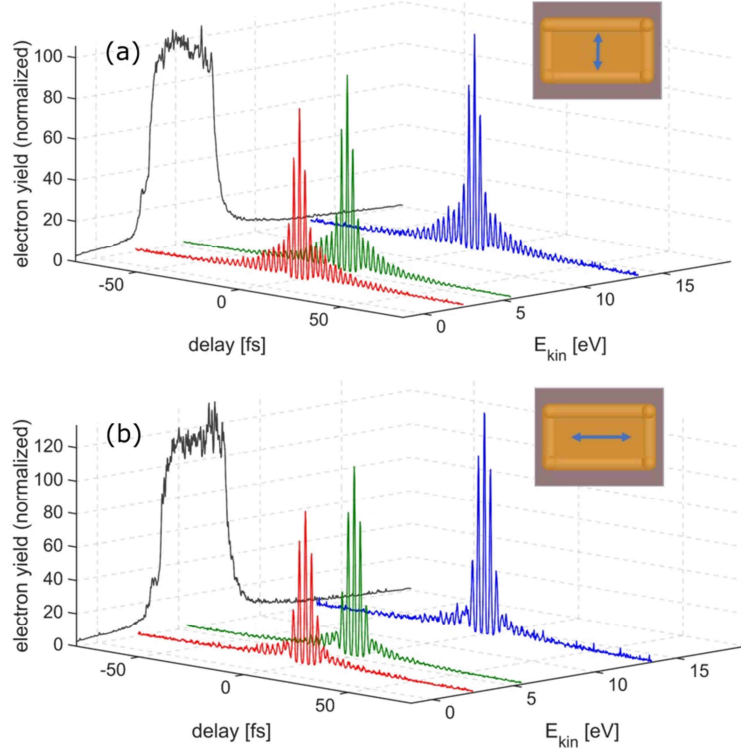
Figure 3. Electron autocorrelation traces evaluated at different electron energies using laser polarization (a) perpendicular to long edge of the nanorod and (b) parallel to long edge of the nanorod.

We also performed a research project connected to the field of attosecond science. High harmonic generation (HHG) was studied on noble gas targets with different cluster sizes [20]. (Clusters are groups of atoms that usually exist only for short periods of time and under special conditions, such as supersonic jets or flows). High harmonic spectra were measured for different backing pressures and gases (Ar, Xe) as a function of driver pulse ellipticity. Different cluster sizes can be produced by different backing pressures at different noble gases, and the cluster sizes can be measured by light scattering [21].

Since the ellipticity-dependent HHG decay is essentially the same for the different gas-pressure pairs and therefore for different cluster size, we can conclude that the recombination process is dominated by atom-to-itself recollisions irrespective of cluster size and material.

This conclusion was supported by classical electron trajectory simulations in elliptic electromagnetic fields. Based on this simulation the ratio of return events with respect to all events (that is, returns and events when the electron misses the cluster) was calculated. This quantity was called "return fraction" (Figure 4). Based on the FWHM of these return fraction curves provide a rough first estimate on the threshold ellipticity one can expect and since this type of increase of threshold ellipticity which could be originate from cluster to itself recombination process was not observed experimentally, we could rule out this mechanism and therefore the atom-to-itself recombination is dominated.
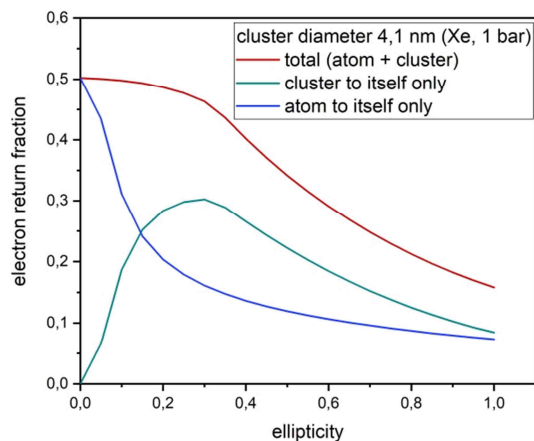
4

Figure 4. Calculated the ratio of return events (return fraction) as a function of ellipticity.. Here, only atom-to-itself and cluster-to-itself events are distinguished.

The realization of those simulations was my major contribution in this publication. For this work I was able to use my previous experience and my own model of plasmonic electron acceleration and electron trajectory computation [22]. Of course, I have adapted this model and simulation to the given problem [20].

References:

[1] M. I. Stockman, M. F. Kling, U. Kleineberg, F. Krausz, "*Attosecond nanoplasmonic-field microscope,",* Nat. Photonics **1**, 539 (2007).

[2] H. A. Atwater; A. Polman, *" Plasmonics for improved photovoltaic devices"*, Nat. Mater, **9**, 205 (2010)

[3] C. Haffner et al. "*Low-loss plasmon-assisted electro-optic modulator*", Nature, **556**, 483 (2018)

[4] A. R. Rastinehad, N. J. Halas et al."*Gold nanoshell-localized photothermal ablation of prostate tumors in a clinical pilot device study*", PNAS, **116**, 18590 (2019)

[5] Falk, A. L. Koppens, F. H. L. Yu, C. L.; Kang, K. de Leon Snapp, N. Akimov, A. V. Jo, M.-H. Lukin, M. D. Park, H. "*Near-field electrical detection of optical plasmons and single-plasmon sources*" Nat. Phys. **5**, 475 (2009).

[6] M. Ono, M. Notomi et al. "*Ultrafast and energy-efficient all-optical switching with graphene-loaded deep-subwavelength plasmonic waveguides*", Nat. Photonics **14**, 37 (2020)

[7] S. Thomas, M. Krüger, M. Förster, M. Schenk, and P. Hommelhoff, " *Probing of Optical Near-Fields by Electron Rescattering on the 1 nm Scale*", *Nano Lett.*, **13** , 4790 (2013)

[8] B. Piglosiewicz, C. Lienau, et al. "*Carrier-envelope phase effects on the strong-field photoemission of electrons from metallic nanostructures*", Nat. Photonics, **8**, 37 (2014)

[9] **P. Dombi,** A. Hörl, **P. Rácz**, I. Márton, A. Trügler, J. R. Krenn, U. Hohenester, "*Ultrafast strong-field photoemission from plasmonic nanoparticles*", Nano Lett., **13**, 674 (2013)

[10] **P. Rácz**, Z. Pápa, I. Márton, J. Budai, P. Wrobel, T. Stefaniuk, C. Prietl, J. R. Krenn and **P. Dombi** *"Measurement of nanoplasmonic field enhancement with ultrafast photoemission,"* Nano Lett, **17**, 1181 (2017)

[11] J. Budai, Z. Pápa, I. Márton, P. Wróbel, T. Stefaniuk, Z. Márton, **P. Rácz**, **P. Dombi,** "*Plasmon-plasmon coupling probed by ultrafast, strong-field photoemission with <7 Angström sensitivity*," Nanoscale **10**, 16261 (2018).

[12] **P. Rácz**, N. Kroó, " *Surface-Plasmon-Assisted Cooper Pair Formation in Ordered Gold Films at Room Temperature*" Phys. Wave Phenom., **27** 192 (2019)

[13] N. Kroó, **P. Rácz**, S. Varró, "*Surface plasmon assisted electron pair formation in strong electromagnetic field*", *EPL,* **105** 67003 (2014)

[14] N. Kroó, **P. Rácz**, S. Varró, " *Surface-plasmon-assisted magnetic anomalies on room temperature gold films in high-intensity laser fields*", *EPL,* **110** 67008 (2015)

[15] Zs. Pápa, P. Sándor, B. Lovász, J. Budai, J. Kasza, Zs. Márton, P. Jójárt, I. Seres, Zs. Bengery, Cs. Németh, **P. Dombi** and **P. Rácz**, „*Control of Plasmonic Field Enhancement by Mode-mixing*" submitted to Appl. Phys. Lett. (see Appendix A)

[16] B. Lovász, P. Sándor, G-Zs. Kiss, B. Bánhegyi, **P. Rácz**, Zs Pápa, J. Budai, C. Prietl, J. Krenn, **P. Dombi,** " *Nonadiabatic tunneling of photoelectrons in plasmonic near-fields*", manuscript to be submitted to Phys. Rev. Lett. 2021 (see Appendix B)

[17] B. Lovász, P. Sándor, Zs. Pápa, B. Éles, B. Bánhegyi, **P. Rácz**, C. Prietl, J. R. Krenn, **P. Dombi**, "*Few-femtosecond plasmon transients probed with nm-scale sensitivity*" The 9th International Conference on Surface Plasmon Photonics (SPP9), Denmark, Copenhagen, 2019

[18] **P. Rácz**, Zs. Pápa, P. Sándor, B. Lovász, B. Bánhegyi, **P. Dombi,** "*Nanooptikai közelterek meghatározása szubnanométeres érzékenységgel*" Magyar Fizikus Vándorgyűlés 2019, Sopron

[19] B. Lovász, P. Sándor, Zs. Pápa, B. Éles, B. Bánhegyi, **P. Rácz,** C. Prietl, J. R. Krenn, **P. Dombi,** "*Few-femtosecond plasmon transients with nm-scale sensitivity*" CLEO Europe 2019 Germany, Munich, 2019

[20] **B. Bódi**, M. Aladi és **P. Rácz**, I. B. Földes és **P. Dombi,** "*High harmonic generation on noble gas clusters*" Opt. Express, **27** 26721 (2019)

[21] M. Aladi, R. Bolla, D.E. Cardenas, L. Veiszb; I.B. Földes " *Cluster size distributions in gas jets for different nozzle geometries* " JINST, **12** C06020 (2017)

[22] **P. Rácz**, V. Ayadi, **P. Dombi,** "*On the role of rescattering and mirror charge in in ultrafast nanooptical field probing with electrons*," J. Opt. **20**, 015501 (2018)

Publications supported by project NKFI FK 125270

[1] J. Budai, Z. Pápa, I. Márton, P. Wróbel, T. Stefaniuk, Z. Márton, **P. Rácz**, **P. Dombi,** "*Plasmon-plasmon coupling probed by ultrafast, strong-field photoemission with <7 Angström sensitivity*," Nanoscale **10**, 16261 (2018). IF: 6.97

[2] **P. Rácz**, N. Kroó, " *Surface-Plasmon-Assisted Cooper Pair Formation in Ordered Gold Films at Room Temperature*" Phys. Wave Phenom, **27** 192 (2019) IF:0.745

[3] **B. Bódi,** M. Aladi és **P. Rácz**, I. B. Földes és **P. Dombi,** "*High harmonic generation on noble gas clusters*" Opt. Express, **27** 26721 (2019) IF: 3.67

[4] Zs. Pápa, P. Sándor, B. Lovász, J. Budai, J. Kasza, Zs. Márton, P. Jójárt, I. Seres, Zs. Bengery, Cs. Németh, **P. Dombi** and **P. Rácz**, „*Control of Plasmonic Field Enhancement by Mode-mixing*" submitted to Appl. Phys. Lett 2021. (see Appendix A)

[5] B. Lovász, P. Sándor, G-Zs. Kiss, B. Bánhegyi, **P. Rácz**, Zs Pápa, J. Budai, C. Prietl, J. Krenn, **P. Dombi,** " *Nonadiabatic tunneling of photoelectrons in plasmonic near-fields*", manuscript to be submitted to Phys. Rev. Lett. 2021 (see Appendix B)

[6] B. Lovász, P. Sándor, Zs. Pápa, B. Éles, B. Bánhegyi, **P. Rácz**, C. Prietl, J. R. Krenn, **P. Dombi**, "*Few-femtosecond plasmon transients probed with nm-scale sensitivity*" The 9th International Conference on Surface Plasmon Photonics (SPP9), Denmark, Copenhagen, 2019

[7] **P. Rácz**, Zs. Pápa, P. Sándor, B. Lovász, B. Bánhegyi, **P. Dombi,** "*Nanooptikai közelterek meghatározása szubnanométeres érzékenységgel*" Magyar Fizikus Vándorgyűlés 2019, Sopron

[8] B. Lovász, P. Sándor, Zs. Pápa, B. Éles, B. Bánhegyi, **P. Rácz,** C. Prietl, J. R. Krenn, **P. Dombi,** "*Few-femtosecond plasmon transients with nm-scale sensitivity*" CLEO Europe 2019 Germany, Munich,

Appendix A:

Control of Plasmonic Field Enhancement by Mode-mixing

Zsuzsanna Pápa[1,2], Péter Sándor[1], Béla Lovász[1], Judit Budai[2], József Kasza[2], Zsuzsanna Márton[2], Péter Jójárt[2], Imre Seres[2], Zsolt Bengery[2], Csaba Németh[1], **Péter Dombi[1,2] and Péter Rácz[1]**

[1] *Wigner Research Centre for Physics, Konkoly-Thege M. ut 29-33, 1121 Budapest, Hungary*
[2] *ELI-ALPS, ELI-HU Non-Profit Ltd., Wolfgang S. u. 3, 6728 Szeged, Hungary*
Corresponding author e-mail address: papa.zsuzsanna@wigner.hu

Abstract: We demonstrate experimentally that nanoscale control of plasmonic field enhancement becomes available by changing the polarization state of light. This is revealed by photoelectron emission from plasmonic nanorods illuminated with linearly and circularly polarized femtosecond laser pulses. Simulations show that the tunability of the field enhancement originates from the mode-mixing property of circularly polarized illumination, meaning parallel excitation of multiple plasmon modes of the nanostructures. This happens with the kinetic energy scaling laws remaining the same.

The localization of optical near-fields at metal nanostructures is exploited in many applications, including sensing [1], ultrafast nanoemitters [2, 3] and optoelectronic device technology [4]. Special attention has been paid to the nanoscale control of localized fields induced by femtosecond laser pulses in metallic nanostructures, such as nanocubes [5-7], nanodisks [8, 9], nanotriangles [10] or more complex geometries [11, 12]. These experiments were mainly carried out with linearly polarized laser pulses. Analysis of plasmonic response and ultrafast electron dynamics induced by circularly polarized light is expected to provide further possibilities regarding the nanoscale control of the electric field. Furthermore, majority of recent work aimed at the visualization of plasmonic near-fields with microscopic methods where the location of the hot spots could be identified and controlled, but the exact value of the field enhancement in the given hot-spots remained unknown.

Determination of the exact field enhancement factor became available [13-15] with our ultrafast method based on the measurement of the kinetic energy spectra of photoelectrons accelerated in the plasmonic near-fields [16, 17]. This technique exploits that the electrons that acquire the highest kinetic energy in the nanolocalized field are the rescattered electrons, the kinetic energy of which scales linearly with the local intensity, based on the ponderomotive acceleration mechanism [13, 18, 19]. Here, we use this method to quantify the field enhancement factor of plasmonic nanorods illuminated by linearly or circularly polarized femtosecond laser pulses. We will show that the same acceleration mechanism and scaling law is valid for both polarization states of the excitation, and the observed differences in field enhancement factors originate from the mode-mixing property of circularly polarized illumination, meaning parallel excitation of multiple plasmon modes of the

nanostructures. Our experiments offer an ultrafast tool for manipulating the field enhancement property of nanostructures by changing the polarization state of light.
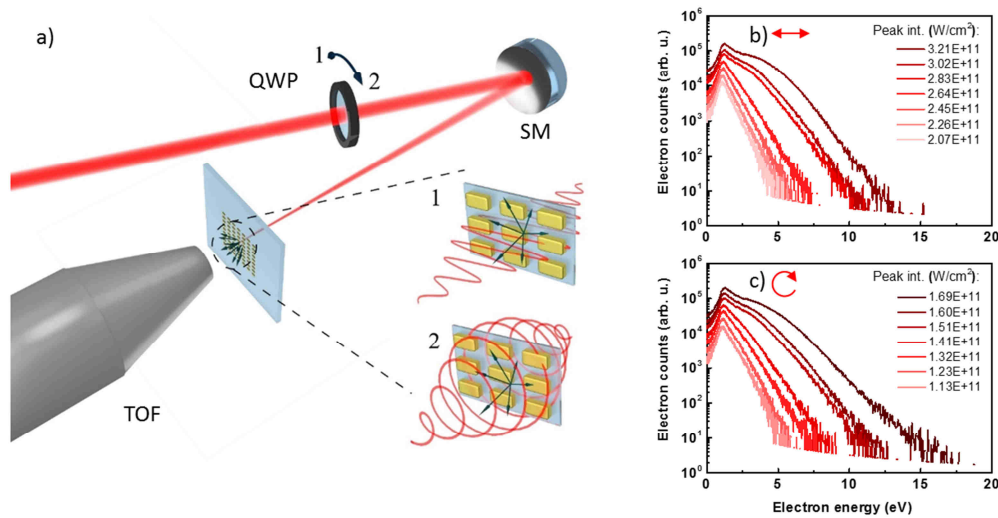

Figure 1: a) Scheme of the experimental setup. Femtosecond laser pulses are guided through a quarter-wave plate (QWP) for adjusting their polarization state (1 – linear, 2 – circular polarization), and subsequently they are focused onto the sample with a spherical mirror (SM). Photoelectrons (marked with green arrows) are collected with a time-of-flight spectrometer (TOF). b) and c) Measured typical electron spectra belonging to 240 nm long nanorods illuminated with femtosecond laser pulses having b) linear and c) circular polarization states.

Plasmonic nanorod samples having different lengths (210, 240, 270 and 300 nm) and different plasmonic extinction maxima (1030, 1115, 1200 and 1275 nm, respectively, see Supplemental Material) were fabricated by electron beam lithography onto indium-tin-oxide (ITO) coated fused-silica plates (details of sample fabrication are provided in Supplemental Material). These samples were placed into a vacuum chamber (pressure below 10^{-7} mBar) and were illuminated from the backside by 30-fs pulses of a fiber laser system operating at the ELI-ALPS facility (central wavelength: 1030 nm, repetition rate: 100 kHz) [20]. Laser pulses were guided through a rotatable quarter-wave plate for adjusting the polarization state, and they were focused by a spherical mirror onto the surface of the nanostructured sample, where photoemission took place (Fig. 1 a)). Photoemitted electrons were collected by a time-of-flight (TOF) spectrometer (Stefan Kaesdorf, ETF11), which has a flight tube of 35 cm, and an acceptance angle of 45° full cone. The axis of the flight tube was normal to the sample surface. By measuring the energy spectra of photoemitted electrons, we could accurately determine maximum kinetic energies (Q_{max}) of these photoelectrons acquired in the rescattering process, which differed remarkably for linearly and circularly polarized pulses (Fig. 1 b) and c)).

Polarization state can significantly affect photoelectron motion. For gas targets, the rescattering processes are mostly suppressed under illumination by circularly polarized light because the electrons do not return to the parent ion [21, 22]. However, in the case of a freestanding nanotip, the electron dynamics under circularly polarized light was shown to be similar to that under linearly

9

polarized light according to the results of Yanagisawa et al. [23]. Therefore, as a first step of the evaluation, we investigated the acceleration process and the achievable electron energies for our samples in the frame of trajectory calculations.

The simulation of the electron trajectories was accomplished within the simple-man model, where electrons are first photoemitted and then become ponderomotively accelerated in the total field (sum of the external and induced fields) of the nanoparticle [24]. For these calculations, the temporal evolution and spatial distribution of the electric field components were extracted from finite-difference time-domain (FDTD) simulations, and the equation of motion was solved in this decaying near-field around the nanorods' hot spots (field distribution examples for 240 nm long nanorod are shown in Fig. 2 a) and b)). Fig. 2 c) and d) show the resulting final kinetic energy of electrons without rescattering (direct electrons) and with rescattering, in units of the ponderomotive energy of the near-field. Kinetic energy is plotted as a function of the time instant of the emission measured from the beginning of the half optical cycle of the local field oscillations which produces the maximum electron energies. For near-infrared, linearly polarized excitation, the scaling of the maximum electron energy during the acceleration in nanooptical near-fields reproduces the literature results rather accurately [13, 19, 25, 26], given that, in this spectral range, the quiver amplitude of the photoelectron motion is much smaller than the decay length of the plasmonic near-field [26]. This criterion is fulfilled under our measurement conditions. Based on these, the $10U_p$ scaling is valid for the maximum kinetic energies of the rescattered electrons. It should be noted here, that U_p is defined throughout this paper using the parameters of the local field and not the exciting laser field:

$$U_p = \frac{e^2 E_{loc,max}{}^2}{4m\omega^2},\qquad\qquad (1)$$

where m and e are the electron mass and charge, respectively, ω is the angular frequency of the local field, E_{loc} is the local electromagnetic field and c is the speed of light.

More importantly, there is only a negligible difference in the energy scaling between circularly and linearly polarized excitation (Fig. 2 d). These results clearly demonstrate that in the case of circularly polarized excitation, the $10U_p$ scaling is also valid, and it can be used during the evaluation of the measured electron spectra.
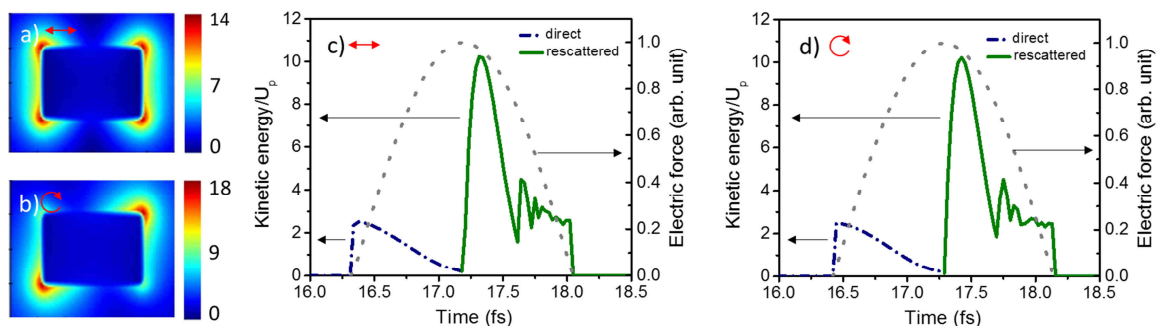

Figure 2: a) and b) Calculated field distribution around a 240 nm long nanorod in a plane containing the hot-spot considering a) linearly or b) circularly polarized illumination. Color bar represents field enhancement factors for the 1030 nm spectral component. c) and d) The final kinetic energy of electrons without rescattering (blue dash dot lines) and with rescattering (green solid lines) relative to the ponderomotive energy in the case of c) linearly polarized and the d) circularly polarized

excitation of the plasmonic field, plotted as a function of emission time. The electric force component that is normal to the surface is also shown as a function of time (gray dotted line).

As a next step, we evaluated the experimental electron spectra measured on the nanorod samples for determining plasmonic field enhancement factors [14]. The measurements showed that in most cases it is the circularly polarized illumination that results in a higher field enhancement factor, with a maximal value belonging to the 240 nm rod (FE_{max}=16.6, see Fig. 3 a)), and with differences larger than 24% for the 270 and 300 nm rods. The measured field enhancement values are in good agreement with the ones extracted from FDTD calculations within the error bars (Fig. 3 b)). Since the trajectory calculations did not show any remarkable difference between the acceleration processes for linear or circular polarization, it is the plasmonic response of the nanorods and the emerging near-fields themselves that should be different under different illumination conditions. Detailed analysis of plasmonic resonance spectra of the nanorods revealed that although the plasmonic response of the nanorods differ only slightly in the spectral range of the laser source (i. e. resonance peak positions are the same for both polarization states, see Supplemental Material), there are prominent differences outside this spectral range affecting the overall behavior. Fig. 3 c) shows the extinction curves for linear and circular polarization considering 240 nm nanorod length. The peak belonging to the plasmon mode along the 240 nm length appears in both curves, while for circular polarization a second peak is visible, which is attributed to the perpendicular plasmonic mode [27]. Although this second peak lies outside the laser spectrum, its effect slightly increases the width and the amplitude of the resonance curve.
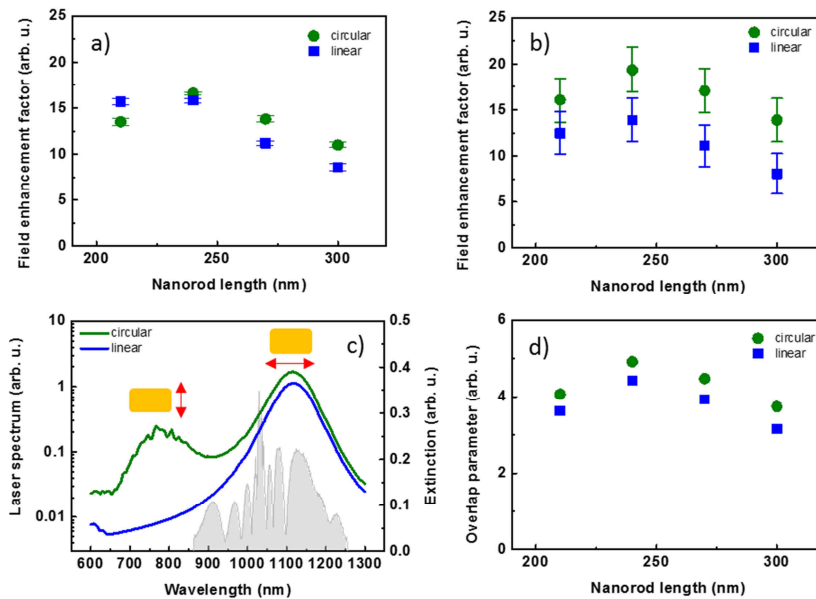

Figure 3: a) Measured maximum field enhancement factor for nanorods having different lengths applying illumination with different polarization states. b) Calculated field enhancement factor using FDTD method. Error bars are calculated considering the broad radius of curvature distribution of the used nanorods. c) Spectrum of the laser source (gray area) and extinction curves belonging to the 240 nm long nanorod. Double peak belonging to the circularly polarized excitation indicates the excitation of different plasmon modes. d) Overlap parameter for nanorods having different lengths considering illumination with different polarization states.

This mode-mixing property of the circularly polarized illumination and its effect on the resonance curve seem to promote a more effective energy transfer between the laser field and the plasmonic modes. To quantify this effectiveness, we determined the spectral overlap between the laser spectrum and the extinction spectra [28] by multiplying the laser spectrum with each extinction spectrum and integrating these product curves. In Fig. 3 d), the spectral overlap parameter is plotted for the different nanorods and different polarization states, showing a clear correlation with the measured field enhancement factors. The similar tendencies observed here support that for circular polarization, it is the excitation of multiple plasmon modes that affects the overall plasmonic response, and - for the geometrical parameters of our nanostructures - results in a higher field enhancement factor. Deviations for the 210 nm nanorod may originate from phase effects, since overlap parameter does not account for phase relations of the two plasmonic modes.

In summary, we showed that polarization tuning of the illuminating laser pulse provides an ultrafast tool for controlling the field enhancement factor of plasmonic nanorods. Our experimental method enabled the determination of field enhancement factors for near-fields induced by linearly and circularly polarized laser pulses. We showed that kinetic energy scaling of the photoelectrons are the same for the applied polarization states, and the differences in the measured field enhancement factors originate from the different plasmonic response of the nanostructures under different illumination conditions. With circularly polarized pulses, multiple plasmonic modes can be excited resulting in a larger overlap between the extinction spectrum of the nanorods and the laser spectrum. This simple mode-mixing property of circularly polarized illumination provides an extra knob to control the near-field of plasmonic nanorods. It can be established easily in experiments and can be further exploited in diverse applications like helicity-driven optical switches with purpose-designed nanostructures.

References

[1] J. N. Anker, W. P. Hall, O. Lyandres, N. C. Shah, J. Zhao, R. P. Van Duyne, "Biosensing with plasmonic nanosensors," Nat. Mater. **7** 442 (2008).

[2] J. Vogelsang, J. Robin, B. J. Nagy, P. Dombi, D. Rosenkranz, M. Schiek, P. Groß, C. Lienau, "Ultrafast Electron Emission from a Sharp Metal Nanotaper Driven by Adiabatic Nanofocusing of Surface Plasmons, " Nano Lett. **15** 4685 (2015).

[3] P. Dombi, Z. Pápa, J. Vogelsang, S. V. Yalunin, M. Sivis, G. Herink, S. Schäfer, P. Groß, C. Ropers, and C. Lienau, "Strong-field nano-optics," Rev. Mod. Phys. **92** 025003 (2020).

[4] D. M. Koller, A. Hohenau, H. Ditlbacher, N. Galler, F. Reil, F. R. Aussenegg, A. Leitner, E. J. W. List, J. R. Krenn, "Organic plasmon-emitting diode," Nat. Photonics **2** 684 (2008).

[5] S. Mazzucco, N. Geuquet, J. Ye, O. Stephan, W. Van Roy, P. Van Dorpe, L. Henrard, M. Kociak, "Ultralocal Modification of Surface Plasmons Properties in Silver Nanocubes," Nano Lett. **12** 1288 (2012).

[6] O. Nicoletti, F. de la Pena, R. K. Leary, D. J. Holland, C. Ducati, P. A. Midgley, "Three-dimensional imaging of localized surface plasmon resonances of metal nanoparticles," Nature **502** (7469) 80-4 (2013).

[7] E. Marsell, R. Svärd, M. Miranda, C. Guo, A. Harth, E. Lorek, J. Mauritsson, C. L. Arnold, H. Xu, A. L'Huillier, A. Mikkelsen, and A. Losquin, "Direct subwavelength imaging and control of near-field localization in individual silver nanocubes," Appl. Phys. Lett. **107** 201111 (2015).

[8] M. Aeschlimann, M. Bauer, D. Bayer, T. Brixner, F. J. Garcia de Abajo, W. Pfeiffer, M. Rohmer, C. Spindler, and F. Steeb, "Adaptive subwavelength control of nano-optical fields, " Nature **446** 301 (2007).

[9] F. P. Schmidt, H. Ditlbacher, F. Hofer, J. R. Krenn, U. Hohenester, "Morphing a Plasmonic Nanodisk into a Nanotriangle," Nano Lett. **14** 8 4810 (2014).

[10] C. Awada, T. Popescu, L. Douillard, F. Charra, A. Perron, H. Yockell-Lelièvre, A.-L. Baudrion, P.-M. Adam, and R. Bachelot, "Selective Excitation of Plasmon Resonances of Single Au Triangles by Polarization-Dependent Light Excitation," J. Phys. Chem. C **116** 14591 (2012).

[11] M. Cinchetti, A. Gloskovskii, S. A. Nepjiko, G. Schonhense, H. Rochholz, and M. Kreiter, "Photoemission Electron Microscopy as a Tool for the Investigation of Optical Near Fields," Phys. Rev. Lett. **95** 047601 (2005).

[12] C. Hrelescu, T. K. Sau, A. L. Rogach, F. Jackel, G. Laurent, L. Douillard, and F. Charra, "Selective Excitation of Individual Plasmonic Hotspots at the Tips of Single Gold Nanostars," Nano Lett., **402** (2011).

[13] P. Dombi, A. Hörl, P. Rácz, I. Márton, A. Trügler, J. R. Krenn, and U. Hohenester, "Ultrafast Strong-Field Photoemission from Plasmonic Nanoparticles," Nano Lett. **13** 674 (2013).

[14] P. Rácz, Z. Pápa, I. Márton, J. Budai, P. Wróbel, T. Stefaniuk, C. Prietl, J. R. Krenn, and P. Dombi, "Measurement of Nanoplasmonic Field Enhancement with Ultrafast Photoemission," Nano Lett. **17** (2) 1181 (2017).

[15] J. Budai, Z. Pápa, I. Márton, P. Wróbel, T. Stefaniuk, Z. Márton, P. Rácz and P. Dombi, "Plasmon-plasmon coupling probed by ultrafast, strong-field photoemission," Nanoscale, **10** 16261 (2018).

[16] P. Dombi, S. E. Irvine, P. Rácz, M. Lenner, N. Kroó, G. Farkas, A. Mitrofanov, A. Baltuška, T. Fuji, F. Krausz, and A. Y. Elezzabi, "Observation of few-cycle, strong-field phenomena in surface plasmon fields," Optics Express, **18** (23) 24206 (2010).

[17] P. Rácz, S. E. Irvine, M. Lenner, A. Mitrofanov, A. Baltuška, A. Y. Elezzabi, and P. Dombi, "Strong-field plasmonic electron acceleration with few-cycle, phase-stabilized laser pulses", Appl. Phys. Lett. **98** 111116 (2011).

[18] M. Busuladzic, A. Gazibegovic-Busuladzic, D. B. Milosevic, "High-order above-threshold ionization in a laser field: Influence of the ionization potential on the high-energy cutoff," Laser Phys. **16** 289 (2006).

[19] S. Thomas, M. Krüger, M. Förster, M. Schenk, P. Hommelhoff, "Probing of Optical Near-Fields by Electron Rescattering on the 1 nm Scale," Nano Lett. **13** 4790 (2013).

[20] S. Hädrich, M. Kienel, M. Müller, A. Klenke, J. Rothhardt, R. Klas, T. Gottschall, T. Eidam, A. Drozdy, P. Jójárt et al., "Energetic sub-2-cycle laser with 216 W average power," Opt. Lett. **41** 4332 (2016).

[21] A. N. Pfeiffer, C. Cirelli, M. Smolarski, D. Dimitrovski, M. Abu-samha, L. B. Madsen, and U. Keller, "Attoclock reveals natural coordinates of the laser-induced tunnelling current flow in atoms, " Nat. Phys. **8** 76 (2012).

[22] B. Bódi, M. Aladi, P. Rácz, I. B. Földes, and P. Dombi, "High harmonic generation on noble gas clusters," Opt. Express **27** 26721 (2019).

[23] H. Yanagisawa, T. Greber, C. Hafner, and J. Osterwalder, "Laser-induced field emission from a tungsten nanotip by circularly polarized femtosecond laser pulses," Phys. Rev. B **101** 045406 (2020).

[24] P. B. Corkum, "Plasma perspective on strong field multiphoton ionization," Phys. Rev. Lett. **71**(13) 1994 (1993).

[25] S.V. Yalunin, G. Herink, D. R. Solli, M. Krüger, P. Hommelhoff, M. Diehn, A. Munk, C. Ropers, "Field localization and rescattering in tip-enhanced photoemission" Ann. Phys. **525** 12 (2012).

[26] G. Herink, D. R. Solli, M. Gulde, C. Ropers, "Field-driven photoemission from nanostructures quenches the quiver motion," Nature **483** 190 (2012).

[27] L. S. Slaughter, W.-S. Chang, P. Swanglap, A. Tcherniak, B. P. Khanal, E. R. Zubarev, S. Link, "Single-Particle Spectroscopy of Gold Nanorods beyond the Quasi-Static Limit: Varying the Width at Constant Aspect Ratio," J. Phys. Chem. C **114** 4934 (2010).

[28] Z. Pápa, J. Kasza, J. Budai, Z. Márton, Gy. Molnár, and P. Dombi, "Tuning plasmonic field enhancement and transients by far-field coupling between nanostructures," Appl. Phys. Lett. **117** 081105 (2020).

Appendix B:

Nonadiabatic tunneling of photoelectrons in plasmonic near-fields

Béla Lovász*[1], Péter Sándor*[1], Gellért-Zsolt Kiss[1,2], Balázs Bánhegyi[1], **Péter Rácz[1]**, Zsuzsanna Pápa[1,3], Judit Budai[3], Chrsitine Prietl[4], Joachim Krenn[4], **Péter Dombi[1,3]**

Affiliations

[1]*Wigner Research Centre for Physics, 1121 Budapest, Hungary*
[2]*National Institute for Research and Development of Isotopic and Molecular Technologies, 400293 Cluj-Napoca, Romania*
[3]*ELI-ALPS Research Institute, ELI-HU Nonprofit Kft., 6720 Szeged, Hungary*
[4]*Institut für Physik, Karl-Franzens-Universität, Graz, Austria*

Abstract - Nonadiabatic tunneling in the transition region between the multiphoton emission (MPE) and adiabatic tunnel emission (TE) regions is experimentally and theoretically explored in the near-fields of plasmonic nanostructures. Measured photoemission spectra clearly show strong-field electron acceleration and recollision in the external field, yet, counterintuitively, the measured photoemission yield shows nonlinear intensity dependece characteristic for MPE. Measured electron spectral features in this transition region were well reproduced with the numerical solution of the time-dependent Schrödinger equation.

Even though Keldysh's original paper [1] laid the theoretical groundwork for much of today's investigations of strong-field physics for both atomic *and* solid state systems, strong-field phenomena were initially explored mostly in atomic and molecular physics scenarios [2]. Investigation of photoemission in intense fields picked up pace slower in the condensed matter physics community. Regardless, in either class of systems, the Keldysh scale parameter is meant to provide a guide to the nature of the photo-ionization or -emission mechanism, expressedly in the limiting cases. For higher optical frequencies and moderately strong fields, with the scale parameter being well above one ($\gamma \gg 1$), multi-photon-induced photoemission dominates, with the photocurrent following the intensity envelope of the laser pulse, raised to the multiphoton order [3]. Upon decreasing the optical frequency and/or increasing the laser intensity ($\gamma \ll 1$), tunneling of the electrons takes over with the photocurrent being ejected adiabatically with the oscillating field into the continuum [3]. However, this general understanding of fundamental light-matter interaction processes does not involve any quantitative prediction (i) either on the value of γ (in other words, the value of the laser intensity) where the transition takes place, (ii) or on the exact physical processes taking place in the transition regime. Here, we show results that provide answers to both of these issues.

Even though some contemporary experiments in atomic and molecular physics [4,5,6,7] and also nanooptics [8] are conducted in the intensity range between these two extremes, systematic experimental research highlighting the nature of this transition itself is missing.

There are a few works where one can follow some sort of evolution of the electron emission and rescattering process as the Keldysh parameter is tuned, but either the tuning is implicit and hence not transparent [9], or it is explicit but it is confined to a region where only one emission process dominates [10,11]. The question naturally arises: where do the transitions between adiabatic and nonadiabatic tunneling, or between nonadiabatic tunneling and MPE take place? For the latter, theoretical work on 1D and 2D H-atom-like systems [12,13] analyzed the γ value for such a transition, putting it to ~2. A combined experimental/theoretical work with gold nanotips confirmed this estimate [14] contributing to the unified picture of laser-atom and laser-solid interactions. A further study [8] links the onset of a delayed emission mechanism from a tungsten tip to that of AC tunneling at $\gamma \approx 2.3$. Based on the analysis of a quantum model of a 1D solid interface, a simple formula ($\gamma \approx 1.18\sqrt{W(eV)}$) was proposed for the lower bound of the transition between the multiphoton and tunneling regimes [15]; resulting in $\gamma =2.5$ for tungsten and 2.7 for gold. In contrast, Ref. [16] reported on the multiphoton-tunnel transition taking place at $\gamma \approx 0.9$.

Here, we demonstrate photoemission between the regimes of multi-photon-induced photoemission and the nonadiabatic tunneling of electrons at the surface of metal nanoparticles. We exploit plasmonic methods enabling nanometer-scale field localization and enhancement [17,18] as well as near-field probing at the same time [19,20,21]. We analyze distinct plateau-like structures that appear in the photoelectron spectra. Even though analogous plateau features have been observed in the high-order above-threshold ionization spectra of atoms [4], however, the electron rescattering process is significantly more efficient in case of solid-state systems, making it significantly easier to detect. This way, we will show that in the transition region tunneling and rescattering of electrons take place at the same time when the electron current depends on the photocurrent in a manner that is characteristic for multiphoton-induced emission.

It is known of photoionization processes in atomic physics that in the strong-field regime, where tunneling electron emission sets in, photoelectrons are accelerated in a quasi-classical manner in the laser field, and after rescattering with the parent ion, they can acquire a maximum kinetic energy which is roughly ten times the ponderomotive potential (U_p) of the laser field, i.e. the average kinetic energy of a free electron moved by the field of the laser. After small quantum mechanical corrections, the corresponding simple formula for the measurable maximum electron kinetic energy is given by $E_{cutoff} = 10.01 U_p + 0.538 I_p$ [22], which is generally considered valid for laser-atom interactions with the ionization potential I_p. First, we have to check whether a similar simple relationship can be used in the case of photoemission from metals by replacing the I_p value with the work function, W. For this, we constructed a quantum mechanical model and determined the scaling law that can be applied for our case, i.e., photoemission into plasmonic near-fields. Within our model, we solved numerically the 1D time-dependent Schrödinger equation (TDSE)

$$i\hbar\frac{\partial \Psi(z;t)}{\partial t} = \left[\hat{T} + \hat{V}(z) + \hat{V}_{le}(z;t)\right]\Psi(z;t) \tag{1}$$

by employing a mixed split-operator and Crank-Nicolson approach [23], where for the length-gauge form of the $V_{le}(z;t) = zE_{loc}(z;t)$ electron-laser interaction term we have also included a $Q(z)$ exponentially decreasing function (i.e., $E_{loc}=E_{in}(t)Q(z)$) that was obtained by fitting on

the field enhancement values acquired by Lumerical FDTD [24] runs at a number of $z_i \geq 0$ ($i \in \{1,2,...\}$) discrete distances in the near vicinity of plasmonic nanorods. The incident fields considered for the simulation were Gaussian pulses centered at 800 nm with pulse durations of $\tau = 5.3$ fs at full-width at half-maximum (FWHM) intensity. Here, the $\Psi_0 = \Psi(z;t=0)$ initial wavefunction (WF) of the electron, located on the Fermi-level in the bulk and described by the $V(z) = \exp[-\beta(z + |z|)] [2(z + |z|) + 1/(E_F + W)]^{-1}$ potential, was obtained by diagonalizing the field-free $H_0 = T + V$ Hamiltonian-matrix represented on a finite difference grid (for more details see the supplementary text).
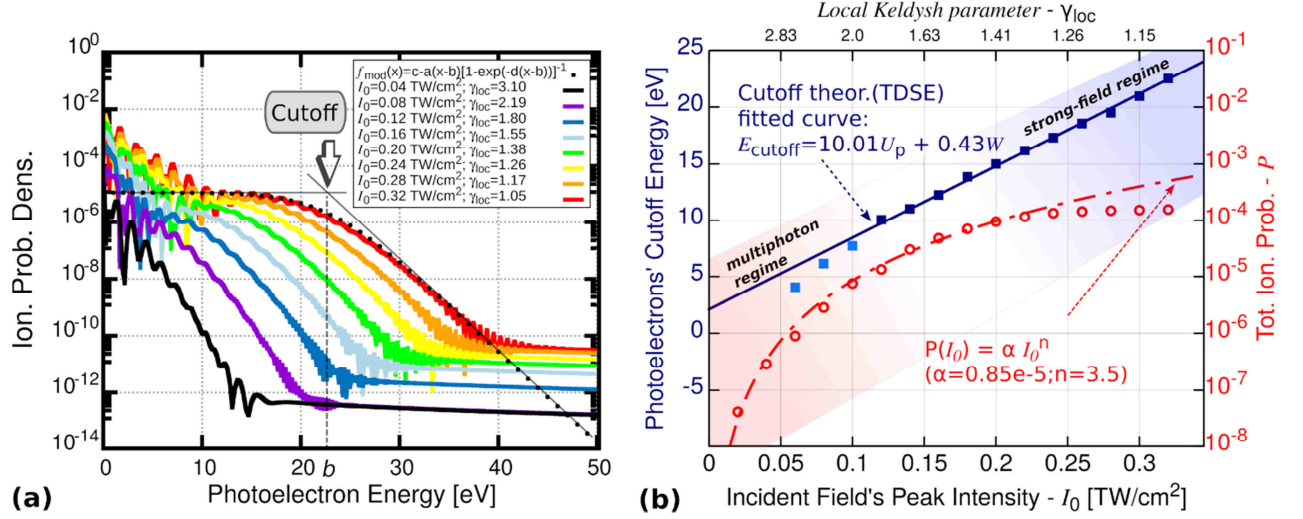
Figure 1. (a) Calculated photoelectron spectra (*ionization probability density*) for different I_0 incident peak intensities 800 nm central wavelength, 5.3 fs pulse length; and 5.3 eV work function (gold). Field enhancement is taken into account with a $Q(z)$ exponentially decaying curve (i.e. for $z \geq 0$ $I_{0,loc}(z) = Q^2(z) I_0$ determines local peak intensities). The electron spectral cutoff energy is defined as the parameter b of the f_{mod} model function that fits the higher energy (*plateau-rolloff*) region. **(b)** The upper solid dark-blue curve shows the scaling of these cutoff energies (solid blue squares) with the incident peak intensity: $E_{cutoff} = 10.01 U_p + 0.43 W$ (with $U_p \sim I_{0,loc,max} \sim I_0$). The scaling follows atomic physics results very well, showing the onset of rescattering for $I_0 > 0.1$ TW/cm^2. In the lower part, final ($t=\tau$) total ionization probabilities (red symbols) are shown together with the $P(I_0) \sim I_0^{3.5}$ power function (dashed red line).

Figure 1(a) shows the photoelectron spectra (projections of the ionized WF onto continuum plane wave states) calculated after the completion of the laser pulse for different I_0 peak field intensities. As one can observe, a clearly distinguishable plateau feature started to appear from $I_0 \geq 0.12$ TW/cm^2. By introducing the concept of the local Keldysh parameter γ_{loc}, which is defined by using the maximum of the plasmonically enhanced local field on the target's surface ($z=0$), i. e., $\gamma_{loc} = \omega(2W)^{1/2}/E_{loc,max}$, with $E_{loc,max} = E_0 Q(z=0)$, one can observe in Fig. 1 that the aforementioned intensity values correspond to $\gamma_{loc} \leq 1.8$. For the higher energy part (the plateau and the roll-off region) of these spectra, we fitted a four-parameter model function $f_{mod}(x) = c - a(x-b)[1-\exp(-d(x-b))]^{-1}$ [dotted line in Fig. 1(a)], where we took the value of the b parameter, i.e., the intersection point of the two linear $\lim_{\varepsilon \to \mp\infty}(f_{mod})$ asymptotes, as the photoelectron cutoff energy: $E_{cutoff} = b$. In Figure 1(b) we show the

obtained cutoff energy values as a function of different peak intensities. By fitting, we determined the scaling

$$E_{cutoff} = 10.01 U_P + 0.43W \qquad (2).$$

It is worth noting here that the last quantum mechanical correction term was found to be only slightly different from the $0.538W$ value obtained for atomic targets [25]. This slight lowering effect of the cutoff energy can be presumably attributed to the decaying profile of the local field in the case of the plasmonic nanotargets, whereas in [25] a homogeneous EM field was considered. Using a decaying field the distant part of the photoelectron's quantum mechanical WF is accelerated by a different, i.e., a lower, electric field than in the regions close to the surface of the metal.

In addition to the scaling law of the cutoff energy we also calculated the final total ionization probability as a function of I_0 (red circles in Fig. 1(b)) and a transition from multiphoton to strong-field regime could be clearly identified starting from the local Keldysh parameter of $\gamma_{loc} \leq 1.4$. In addition to this, by considering that the plateau feature started to appear in the spectra from $\gamma_{loc} \leq 2$, we showed that the transition between the two regimes starts within the region of $\gamma_{loc} \in [1.4, 2]$, providing a reliable estimate and initial answer to one of our fundamental research questions.

After having a verified simple scaling law at hand (Eq. 2), we could study how photoemission from different plasmonic nanoparticles takes place into electromagnetic hotspots of our samples. We used laser pulses with octave-spanning bandwidth that were generated by a commercial Ti:sapphire laser oscillator (Venteon Pulse One) at a repetition rate of 80 MHz. The pulses were compressed to ~7.2 fs duration in case of sample A (see table 1) and 10.7 fs for samples B and C by a combination of chirped mirrors (Layertec 103366), a pair of fused silica wedges and plane-parallel fused silica slabs. Characterization of the pulse duration was performed using interferometric FROG (IFROG) and d-scan techniques (see inset of Fig. 2(a)). The laser pulse energy was controlled by a neutral density filter
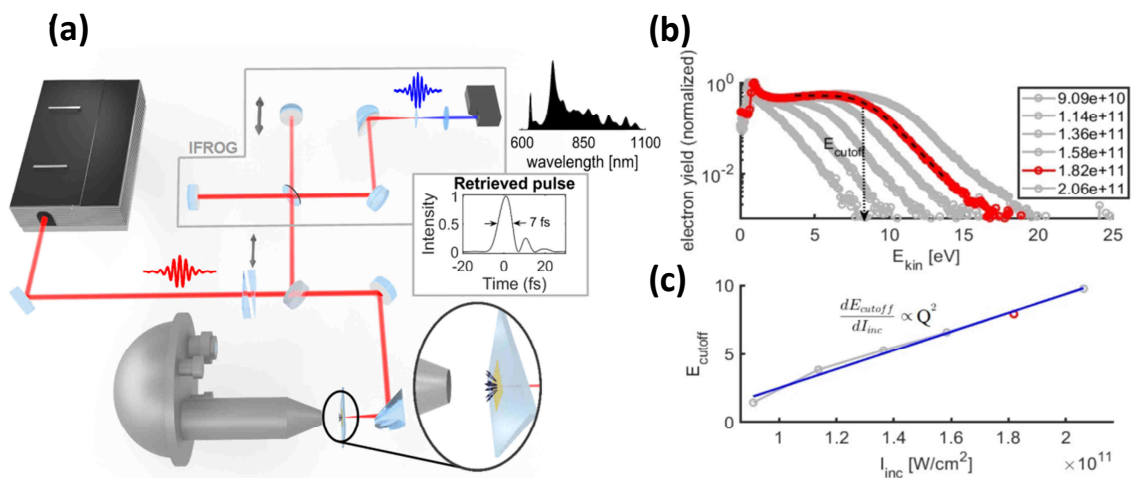
Fig. 2. (a) Scheme of the experimental setup. Few-cycle laser pulses from the a Ti:S oscillator are focused by an off-axis parabolic mirror and illuminate the back side of the sample. Photoemitted electrons are detected by a hemispherical energy analyzer. Insets:

measured laser spectrum and reconstructed temporal pulse profile in case of sample A.
(b) Typical measured photoemission spectra for different laser intensities (the values are given in the legend in W/cm^2). **(c)** Cutoff energies extracted from the spectra.

The sample was housed in a high-vacuum chamber (base pressure: <10^{-7} mbar), and was positioned with nm accuracy in all three dimensions using stacked piezostages (Attocube ECS 3030). Laser pulses with linear polarization were focused to a spot of ~7.4 µm in diameter (1/e^2) with an off-axis parabolic mirror, and illuminated the sample from the back side. Electrons emitted from the surface of the nanostructures entered a hemispherical energy analyzer (SPECS Phoibos 100 R7). Data acquisition was controlled using the SpecsLab Prodigy software, by setting an energy width of 0.1 eV and scanning center of the energy window between 0.4 eV and typically 50 eV. The spectra shown on top right inset of Fig. 2 was collected with an entry slit width of 3 mm and an open exit slit. To avoid detector saturation, the signal was reduced by a factor of 20-30 by using a laser beam chopper to let only a small portion of the pulses through to the experiment. The Earth's ambient magnetic field is compensated with 3 sets of Helmholtz coils, seated outside of the vacuum chamber.

For a given nanostructure, a series of spectra were collected at different incident laser intensities. At low laser intensities, the spectra show a narrow low-energy peak at around 7-8 eV (due to the instrumental bias of the hemispherical analyzer), and an exponential 'tail' at higher electron kinetic energies (a straight line on a semilogarithmic graph, see Fig. 2(b)). These correspond to direct electrons (i.e. those that are accelerated, but not rescattered in the local fields). As the laser intensity is increased—just like in the simulations—the spectra develop a distinct plateau-like feature at higher electron kinetic energies, signaling the appearance of electrons that are ejected, accelerated and rescattered in the time-varying enhanced local fields. We analyze this portion of the electron energy distributions to determine the strength of the local fields. At each laser intensity, the electron cutoff kinetic energy was determined from the associated spectrum. We substitute the expression for the ponderomotive energy (U_p) to equation (2) to find that the cutoff energy is a linear function of the peak intensity, and its slope is proportional to the square of the nanoplasmonic field enhancement.

$$E_{cutoff} = 10.01 U_P + 0.43W$$
$$= 10.01 \frac{e^2}{4 m_e \varepsilon_0 c \omega^2} Q^2 I_{inc} + 0.43\,W \qquad (3)$$

Here, ω is the central angular frequency of the laser, W is the work function of the metal (~5.3 eV for gold in our case), E_{inc} is the electric field of the incident laser radiation, Q is the local field enhancement ($E_{loc} = Q E_{inc}$), m_e is the electron mass and e is the elementary charge. We use this relationship to determine the field enhancement by linearly fitting the cutoff energy vs. peak intensity curve. (See Figs. 2(b) and 2(c) for illustration and the supplementary information for details of this procedure.)

Fig. 3 shows the overview of the results. In panels (a-c) we show SEM images of the nanostructures A, B, and C ☐sed in the experiment (for designations, see Table 1; the incident laser field is polarized horizontally, along the scale bar). In each column of Fig. 3, the data corresponding to each nanostructure is present. The photoelectron yield vs incident laser

intensity (bottom axis) are plotted on a double logarithmic scale in panels (j-l). In the same panels, the local Keldysh parameter (γ_{loc}) is indicated (top axis). Linear fit (red solid line) to the raw data (black circles) show slopes between 2.9 and 3.6, indicative of photoelectron emission due to absorption of about 3-4 photons from the incident laser field. These are reasonable numbers given that our laser spectrum spans from 630 nm to 1100 nm with a central wavelength of 803 nm (corresponding to 1.54 eV photons) and the nominal value of 5.3 eV for the work function. These are also in accordance with results of our simulations (see Fig. 1(b)).
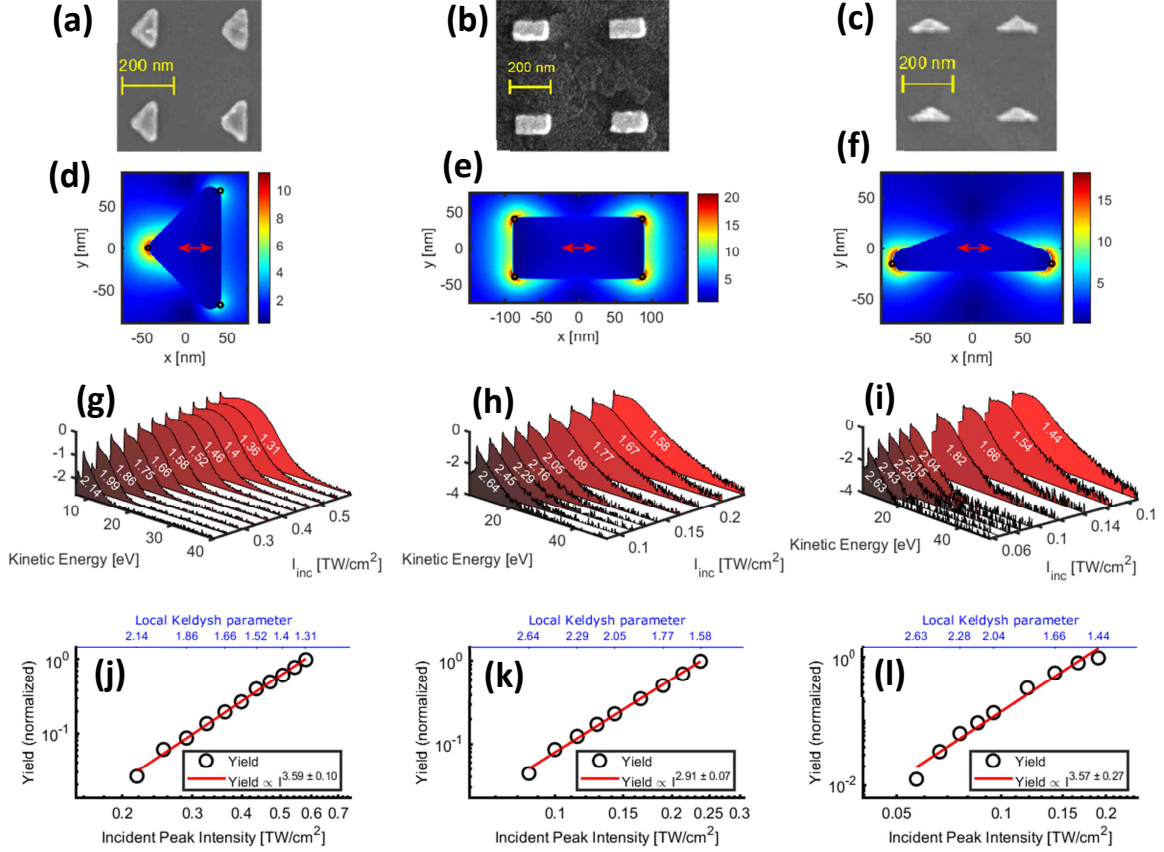
Fig. 3. (a-c) SEM images of the gold nanostructures. The laser polarization was linear, and horizontal along the scalebar in all cases. **(d-f)** Spatial distributions of the field enhancement values from FDTD simulations in a plane at a height of ~15 nm above the substrate surface. Black circles mark monitor points in these planes; these and further monitor points in other planes were used for calculating the average field enhancement values in Table 1. **(g-i)** Measured photemission spectra for different incident laser intensities, with the local Keldysh parameter values indicated for each spectrum. (The yield is normalized to the global maximum value of each dataset and shown on a logarithmic scale.) **(j-l)** Photoemission yields as a function of incident peak laser intensity (black circles) and linear fits (solid red lines). The nonlinear exponents are ~3.6 for the triangular nanostructures and ~2.9 for the nanorods.

Photoelectron spectra (see Fig. 3(g-i)) at higher laser intensities give evidence of the appearance of rescattering electrons with substantially increased kinetic energy, which form the above-mentioned plateau-like feature. This results in the cutoff energy also shifting to higher energies, and enables the determination of the field enhancement (see Table 1), along

with the magnitude of the local field and the local Keldysh parameter. Earlier work [16] suggests that in case the quiver amplitude of the electrons is much smaller than the local field decay length (i.e. the adiabacity parameter $\delta > 1$), then the appearance of the plateau electrons signifies that the Keldysh parameter is $\gamma_{loc} < 1$, i.e. tunneling starts to play an important role in the ionization process. The shape of the photoemission spectra shown in Fig. 3(g-i) for the lowest incident intensities consist of a low-energy peak and an exponential fall-off (straight line on the semi-logarithmic plot, hence the spectra are 'triangle-shaped'). Such spectra are well-known to be observed under conditions $\gamma_{loc} \gg 1$, i.e. in the multiphoton regime [26].

As the intensity is increased, high energy electrons start to appear and contribute to the plateau region of the spectrum due to acceleration in the enhanced local field and elastic rescattering from the gold surface. This transition is observed at Keldysh parameter values of about 1.99, 2.29 and 2.28, respectively. This is in very good agreement with our theoretical results in Fig. 1, showing the appearance of $10U_p$ electrons for $\gamma_{loc} < 2.2$, representing the onset of strong-field effects. However, at the same time, for $1.35 < \gamma_{loc} < 2.2$ in the nanoplasmonic near-field, the power-law scaling of the photocurrent with laser intensity also holds true with a constant exponent. Thus, strong-field electron acceleration features and multiphoton scaling laws are present at the same time in this transition region. This is in accord with experiments highlighted in [8], but not with the calculations shown in [15]. In the latter, a hallmark of the onset of tunnel emission is the deviation from the smooth power-law dependence. Our work highlights the importance of considering the spectral signatures of the rescattered electrons, in addition to the dependence of the emitted yield on peak intensity.

Nanostructure		Field Enhancement	
		measured	calculated
A	Triangle (160 nm x 100 nm), fig. 3(a)	9.4 ± 0.63	8.28 ± 2.2
B	Rod (192 nm x 103 nm) , fig. 3(b)	12.2 ± 0.3	10.7 ± 1.8
C	Triangle (50 nm x 200 nm) , fig. 3(c)	15 ± 0.6	13.8 ± 1.3

Table 1. Summary of the measured and calculated field enhancement values (see supplementary information for details).

In summary, we demonstrated nonadiabatic tunneling photoemission in few-cycle near-fields in the vicinity of various plasmonic nanostructures. By doing so, we pointed out the regime where multiphoton emission scaling laws and strong-field electrons are present at the same time. By analyzing these electron spectra and determining plasmonic field enhancement with spectral cutoffs, we could show the presence of ponderomotively accelerated electrons in this region which is perfectly characterized by multiphoton emission scaling laws. This way, we could also show the Keldysh-gamma range where nonadiabatic tunneling photoemission takes place.

References

[1]   L. V. Keldysh, *Ionization in the Field of a Strong Electromagnetic Wave*, Sov. Phys. JETP **122**, 449 (2016).

[2]   H. G. Muller, P. Agostini, G. Petite, R. R. Freeman, P. H. Bucksbaum, W. E. Cooke, G. Gibson, T. J. Mcilrath, L. D. van Woerkom, T. F. Gallagher, P. B. Corkum, N. H. Burnett, F. Brunel, A. L'Huillier, L.-A. Lompre, G. Mainfray, C. Manus, T. S. Luk, A. McPherson, K. Boyer, C. K. Rhodes, K. C. Kulander, K. J. Schafer, J. L. Krause, J. H. Eberly, R. Grobe, C. K. Law, Q. Su, P. Lambropoulos, X. Tang, R. M. Potvliege, R. Shakeshaft, and M. Gavrila, *Atoms in Intense Laser Fields* (Cambridge University Press, Cambridge, 1992).

[3]   G. L. Yudin and M. Y. Ivanov, *Nonadiabatic Tunnel Ionization: Looking inside a Laser Cycle*, Phys. Rev. A - At. Mol. Opt. Phys. **64**, 4 (2001).

[4]   W. Becker, S. P. Goreslavski, D. B. Milošević, and G. G. Paulus, The Plateau in Above-Threshold Ionization: The Keystone of Rescattering Physics, Journal of Physics B: Atomic, Molecular and Optical Physics (2018).

[5]   M. Meckel, D. Comtois, D. Zeidler, A. Staudte, D. Pavičić, H. C. Bandulet, H. Pépin, J. C. Kieffer, R. Dörner, D. M. Villeneuve, and P. B. Corkum, *Laser-Induced Electron Tunneling and Diffraction*, Science Vol 320, Issue 5882 (2008).

[6]   N. Werby, A. Natan, R. Forbes, and P. H. Bucksbaum, *Disentangling the subcycle electron momentum spectrum in strong-field ionization*, Phys. Rev. Research 3, (2021).

[7]   P. Sándor, A. Sissay, F. Mauger, M. W. Gordon, T. T. Gorman, T. D. Scarborough, M. B. Gaarde, K. Lopata , K. J. Schafer, and R. R. Jones, *Angle-dependent strong-field ionization of halomethanes*, J. Chem. Phys. **151**, 194308 (2019).

[8]   H. Yanagisawa, S. Schnepp, C. Hafner, M. Hengsberger, D. E. Kim, M. F. Kling, A. Landsman, L. Gallmann, and J. Osterwalder, *Delayed Electron Emission in Strong-Field Driven Tunnelling from a Metallic Nanotip in the Multi-Electron Regime*, Sci. Rep. **6**, 35877 (2016).

[9]   M. Krüger, M. Schenk, P. Hommelhoff, G. Wachter, C. Lemell, and J. Burgdörfer, *Interaction of Ultrashort Laser Pulses with Metal Nanotips: A Model System for Strong-Field Phenomena*, New J. Phys. **14**, 085019 (2012).

[10]   G. Herink, D. R. Solli, M. Gulde, and C. Ropers, *Field-Driven Photoemission from Nanostructures Quenches the Quiver Motion*, Nature **483**, 190 (2012).

[11]   P. Colosimo, G. Doumy, C. I. Blaga, J. Wheeler, C. Hauri, F. Catoire, J. Tate, R. Chirla, A. M. March, G. G. Paulus, H. G. Muller, P. Agostini, and L. F. Dimauro, *Scaling Strong-Field Interactions towards the Classical Limit*, (2008).

[12] R. Wang, Q. Zhang, D. Li, S. Xu, P. Cao, Y. Zhou, W. Cao, and P. Lu, *Identification of Tunneling and Multiphoton Ionization in Intermediate Keldysh Parameter Regime*, Opt. Express **27**, 6471 (2019).

[13] X. Hao, Z. Shu, W. Li, S. Hu, and J. Chen, *Quantitative Identification of Different Strong-Field Ionization Channels in the Transition Regime*, Opt. Express **24**, 25250 (2016).

[14] R. Bormann, M. Gulde, A. Weismann, S. V. Yalunin, and C. Ropers, *Tip-Enhanced Strong-Field Photoemission*, Phys. Rev. Lett. **105**, 147601 (2010).

[15] M. Pant and L. K. Ang, *Ultrafast Laser-Induced Electron Emission from Multiphoton to Optical Tunneling*, Phys. Rev. B **86**, 45423 (2012).

[16] B. Piglosiewicz, S. Schmidt, D. J. Park, J. Vogelsang, P. Groß, C. Manzoni, P. Farinello, G. Cerullo, and C. Lienau, *Carrier-Envelope Phase Effects on the Strong-Field Photoemission of Electrons from Metallic Nanostructures*, Nat. Photonics **8**, 37 (2014).

[17] L. Novotny and B. Hecht, *Principles of Nano-Optics* (Cambridge University Press, 2006).

[18] S. A. Maier, *Plasmonics: Fundamentals and Applications* (Springer {US}, 2007).

[19] P. Dombi, A. Hörl, P. Rácz, I. Márton, A. Trügler, J. R. Krenn, and Ulrich Hohenester, *Ultrafast Strong-Field Photoemission from Plasmonic Nanoparticles*, Nano Lett. 13, 2, 674–678 (2013).

[20] P. Rácz, Z. Pápa, I. Márton, J. Budai, P. Wróbel, T. Stefaniuk, C. Prietl, J. R. Krenn, and P. Dombi, *Measurement of Nanoplasmonic Field Enhancement with Ultrafast Photoemission*, Nano Lett. **17**, 1181 (2017).

[21] J. Budai, Z. Pápa, I. Márton, P. Wróbel, T. Stefaniuk, Z. Márton, P. Rácz, and P. Dombi, *Plasmon–Plasmon Coupling Probed by Ultrafast, Strong-Field Photoemission with <7 Å Sensitivity*, Nanoscale **10**, 16261 (2018).

[22] S. V. Yalunin, G. Herink, D. R. Solli, M. Krüger, P. Hommelhoff, M. Diehn, A. Munk, and C. Ropers, *Field Localization and Rescattering in Tip-Enhanced Photoemission*, Ann. Phys. **525**, 12 (2013).

[23] J. Crank and P. Nicolson, *A Practical Method for Numerical Evaluation of Solutions of Partial Differential Equations of the Heat-Conduction Type*, Math. Proc. Cambridge Philos. Soc. **43**, 50 (1947).

[24] Lumerical Inc., *Https://Www.Lumerical.Com/Products/*, https://www.lumerical.com/products/.

[25] M. Busuladžić, A. Gazibegović-Busuladžić, and D. B. Milošević, *High-Order above-Threshold Ionization in a Laser Field: Influence of the Ionization Potential on the High-Energy Cutoff*, Laser Phys. **16**, 289 (2006).

[26] P. Lang, X. Song, B. Ji, H. Tao, Y. Dou, X. Gao, Z. Hao, and J. Lin, *Spatial- and Energy-Resolved Photoemission Electron from Plasmonic Nanoparticles in Multiphoton Regime*, Opt. Express **27**, 6878 (2019).